International Journal of Heat and Fluid Flow 81 (2020) 108520

Contents lists available at ScienceDirect

International Journal of Heat and Fluid Flow

journal homepage: www.elsevier.com/locate/ijhff

A study on thrombus influenced red blood cell flow in microvasculature using moving particle semi-implicit method

Ze-Xiao Wang, Jian Guan, Lei Chen*, Wen-Quan Tao

Key Laboratory of Thermo-Fluid Science and Engineering, Ministry of Education; School of Energy & Power Engineering, Xi'an Jiaotong University, Xi'an, Shaanxi 710049, People's Republic of China

ARTICLE INFO

Keywords:
MPS method
RBCs
Microvasculature
Thrombus

ABSTRACT

Microvasculature plays a decisive role on the normal operation of the human body. Previous studies have shown that the causes of microvascular hemolytic anemia and other diseases are closely related to the interaction between micro-thrombi and RBCs. The movement and deformation of Red Blood Cells (RBCs) in microvasculature with hemicyclic micro-thrombi of different sizes on the wall are simulated based on the Moving Particle Semi-implicit method (MPS) and the spring network model of RBCs membrane. Simulation of a single RBC passing the straight blood vessel indicates the strong squeeze of the RBC caused by the thrombus, which leads to a 38.5% increasing of the RBC velocity and a greater deformation, and such squeeze effect is positively related with the size of the thrombus. When two RBCs pass through the straight blood vessel with two thrombi on the both sidewalls, the deformation of the RBCs first increases and then decreases. Results show that when the axial position between the two thrombi is $10 \times d_0$ different, the deformation of RBCs reaches the maximum of 3.10 (upper) and 2.79 (lower), respectively. When two side-by-side RBCs pass through a bifurcated blood vessel with a sidewall thrombus, the velocity and deformation of RBCs are greatly affected by the thrombus. When the thrombus radius changes from $0 \times d_0$ to $20 \times d_0$, the peak velocities of the two cells increase by 51.6% (upper) and 67.9% (lower), respectively.

1. Introduction

The exchange of substances and energy between blood and body fluids is largely based on the microvasculature. Therefore, the flow of blood cells and plasma in the microvasculature plays an important role in human health. Blood is mainly composed by plasma and blood cells including RBCs, white blood cell and platelets, among which RBCs account for about 90% of the blood cells and are the main component of the blood cells (Xiang et al., 2017). Human RBCs are usually in the shape of biconcave dishes (Sui et al., 2008), with the mean diameter of 8 μm (Fedosov et al., 2010). In the actual blood circulation, the smallest part of the microvasculature can only allow one RBC to pass through; when a micro-thrombus exists on the wall of the microvasculature, the diameter of blood vessel becomes smaller, even smaller than the diameter of the RBC, thus the RBC will have greater elastic deformation when it passes through the blood vessel (Sugihara-Seki and Fu, 2005; Suzuki et al., 1996). Experiments (Pries et al., 1989; Schmid-Schönbein et al., 1980; She et al., 2013; Li et al., 2014) show that the rheological properties of the microvasculature are closely related to the deformability of RBCs. Therefore, the deformation characteristics of RBCs cannot be neglected in the numerical simulation of blood flow in the microvasculature.

For now, some methods have been used in computational fluid dynamics (CFD) simulation of blood flow process (Yu et al., 2015; Di Achille et al., 2017; Sharifi and Moghadam, 2016; Ye et al., 2017; Gambaruto, 2015; Tsubota et al., 2006; Discher et al., 1998; Jared et al., 2008; Liu and Liu, 2006; Hosseini and Feng, 2009; Dzwinel et al., 2003; Ye et al., 2018). Traditionally, the finite volume method based on Euler's representation is used in the simulation. This method is suitable for calculating large-scale blood flow (Yu et al., 2015; Di Achille et al., 2017; Sharifi and Moghadam, 2016), where RBCs can only be regarded as rigid particles. If this method is adapted to simulate the deformation of RBC membrane in micro-scale, the dynamic mesh method is needed, which leads to low calculation accuracy. Another relatively new method is the meshless particle method based on Lagrange representation. Particle method can model the elastic force in RBC membrane as the elastic force in fluid particles. It can also deal with the interface between fluid and other phases conveniently. Thus, the interaction between RBCs and plasma in the microvasculature can be simulated more accurately (Ye et al., 2017; Tsubota et al., 2006;

* Corresponding author.
E-mail address: chenlei@mail.xjtu.edu.cn (L. Chen).

https://doi.org/10.1016/j.ijheatfluidflow.2019.108520
Received 30 October 2019; Accepted 27 November 2019
Available online 10 December 2019
0142-727X/

Hosseini and Feng, 2009). Ye et al. (2017) used Smoothed Dissipative Particle Dynamics (SDPD) method to simulate the movement of RBCs in the microvasculature with different levels of curvature. The effect of secondary flow on the movement of RBCs caused by curvature was investigated. Tsubota et al. (2006) used Moving Particle Semi-implicit (MPS) method to simulate the movement of RBCs in straight blood vessels, and the relationship between the velocity of RBCs and the diameters of different blood vessels was also analyzed. Hosseini and Feng (2009) simulated the movement and deformation of RBCs in shear flow and Poiseuille flow based on Smoothed Particle Hydrodynamics (SPH) method, and the relationship between the flexural modulus of cell membrane and cell movement was also studied. These simulation results clearly show the interaction between RBCs and plasma, however, only the movement of a single cell is examined without considering the additional effect of thrombus on RBCs' movement.

Among the existing meshless methods, Moving Particle Semi-implicit method (MPS) acts as a simulation method based on pure Lagrangian formulation, and the explicit algorithm of velocity is combined with the implicit algorithm of pressure, which ensures the calculation accuracy and reduces the calculation time. This method was first proposed by Koshizuka in 1996 and has been widely used in incompressible flows with interfaces including free surface (Tsubota et al., 2006; Koshizuka and Oka, 1996; Sun et al., 2007; Koshizuka et al., 2015; Harada et al., 2007; Sun et al., 2008). In this paper, MPS method is adopted to simulate the process of blood flow through the microvasculature. The distribution of blood flow field and the movement of RBCs are studied when there are hemispherical thrombi with different sizes and locations on the wall of blood vessels. In particular, three different situations are investigated, including a single RBC in a straight micro blood vessel with a single thrombus on the sidewall, two side-by-side RBCs in a straight blood vessel with two thrombi on both sidewalls, and two side-by-side RBCs in a bifurcated blood vessel with a thrombus near the bifurcation point.

2. Simulation method

2.1. Moving particle semi-implicit method

MPS method is adopted to describe plasma (Tsubota et al., 2006; Sun et al., 2007). MPS method is a pure Lagrangian meshless method used for incompressible flow. Its basic idea is to discretize fluid into many fluid particles. The velocity and pressure of the flow field are stored on each particle and follow the motion of each particle (Tsubota et al., 2006; Sun et al., 2007). The plasma can be treated as incompressible flow, thus it satisfies the incompressible Navier–Stokes equation:

$$\begin{cases} \frac{d\rho}{dt} = \frac{\partial\rho}{\partial t} + \cdot(\rho \boldsymbol{u}) = 0 \\ \frac{d\boldsymbol{u}}{dt} = f - \frac{1}{\rho}\nabla p + \upsilon\nabla^2 u \end{cases} \tag{1}$$

Predictor-corrector method is adopted to solve the incompressible Navier–Stokes equation. For each time step k, an intermediate velocity for each particle is first calculated based on the velocity at timestep k of each particle:

$$\boldsymbol{u}^* = \boldsymbol{u}_k + (\boldsymbol{f}_k + \upsilon\nabla^2\boldsymbol{u}_k)\Delta t \tag{2}$$

In this equation, $\boldsymbol{f}_k$ refers to the external force acted on the fluid, and Δt is the timestep length. Then the influence of pressure is calculated based on the Poission Equation, and the intermediate velocity is corrected to obtain the velocity at timestep $k+1$:

$$\boldsymbol{u}_{k+1} = \boldsymbol{u}^* - \frac{\Delta t}{\rho}\nabla p_{k+1} \tag{3}$$

Interaction between two neighboring particles is expressed by a kernel function (4) (Koshizuka et al., 2015), and the kernel function is used in discretizing the differential operators.

$$w(r) = \begin{cases} \frac{r_e}{r} - 1 & (0 \le r \le r_e) \\ 0 & (r > r_e) \end{cases} \tag{4}$$

where, r is the distance between two particles and r_e is the action range of interaction. Based on this kernel function, the differential operators in Navier–Stokes Equation and continuity equation can be expressed in formula (5) and (6) (Koshizuka et al., 2015):

$$\langle\nabla\phi\rangle_i = \frac{d}{n_0}\sum_{j\neq i}\frac{\phi_j - \phi_i}{|\boldsymbol{r}_{ij}|^2}(\boldsymbol{r}_j - \boldsymbol{r}_j)w(|\boldsymbol{r}_{ij}|, r_e) \tag{5}$$

and

$$\langle\nabla^2\phi\rangle_i = \frac{2d}{n_0\lambda_0}\sum_{j\neq i}(\phi_j - \phi_i)w(|\boldsymbol{r}_{ij}|, r_e) \tag{6}$$

where d is the number of spatial dimensions, ϕ is the physical quantity of operator, λ_0 is a constant representing the average square distance between the particles and n_0 is the initial particle number density.

MPS method adopts semi-implicit algorithm. For each time step, the Laplace operator of the current velocity is obtained first, and the external force and viscous terms in Navier–Stokes equation are explicitly calculated. Then, the pressure gradient is calculated implicitly based on the Poission Equation:

$$\nabla^2 p_{k+1} = -\frac{\rho}{(\Delta t)^2}\frac{\langle n^*\rangle - n_0}{n_0} \tag{7}$$

where:

$$\langle n^*\rangle_i = \sum_{j\neq i} w(|\boldsymbol{r}_{ij}^*|, r_e) \tag{8}$$

Using the discretized Laplacian operator, $\nabla^2 p_{k+1}$ can be calculated as:

$$\langle\nabla^2 p_{k+1}\rangle_i = \frac{2d}{n_0\lambda_0}\sum_{j\neq i}(p_j - p_i)w(|\boldsymbol{r}_{ij}^*|, r_e) \tag{9}$$

Combing the discretized Poission Equation for each particle together, a system of linear equations for each p_i can be established. In this work, conjugate gradient method is used to solve that equation.

2.2. Spring network model of RBC membrane

There is no cytoskeleton or nucleus in mature human RBCs, thus their motion characteristics are mainly determined by cell membranes (Nakamura et al., 2014). In meshless method, spring network model is often used to describe the deformation of RBCs (Sui et al., 2008; Ye et al., 2017; Gambaruto, 2015; Tsubota et al., 2006; Ahmadian et al., 2012; Xiao et al., 2013). In this method, cell membranes are discretized into fluid particles connected by spring network to simulate the elastic deformation of cell membranes.

The membrane of RBC is mainly composed of phospholipid bilayer and membrane protein (Imai et al., 2016; Mohandas and Gallagher, 2008). Due to the thickness of the phospholipid bilayer and its strong incompressibility, the cell membrane can, to some extent, resist stretching and bending deformation (Balogh and Bagchi, 2017; Tsubota and Wada, 2010). Therefore, there are two forms of springs in spring network: stretch-compression spring and bending spring (Balogh and Bagchi, 2017; Tsubota and Wada, 2010; Kamada et al., 2012), as shown in Fig. 1.

For fluid particle j in the membrane, the stretch-compression spring force acting between the adjacent membrane particles i and j can be expressed as follows (Imai et al., 2010):

$$\boldsymbol{F}_{ij}^s = k_s(|\boldsymbol{r}_{ij}| - r_0)\frac{\boldsymbol{r}_{ij}}{|\boldsymbol{r}_{ij}|} \tag{10}$$

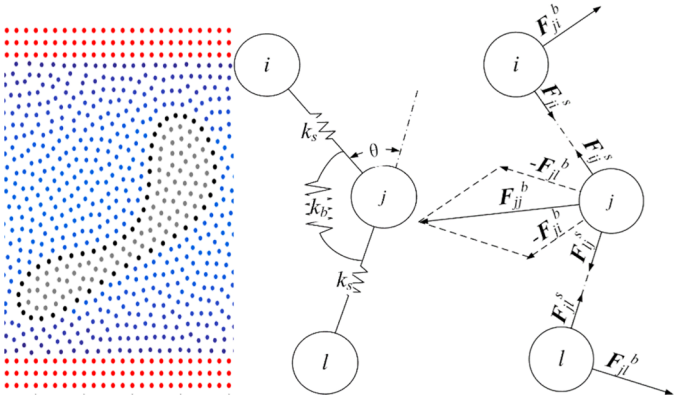

Fig. 1. Diagram of membrane particle spring model.

where r_0 is the original length of the spring, which is generally taken as the initial spacing of particles; k_s is the elastic coefficient of the tension-compression spring. For the three sequential connected particles*i*, *j* and *l*, if *j* is regarded as the center, the force of the bending spring can be expressed as (Imai et al., 2010):

$$\begin{cases} \boldsymbol{F}_{ji}^b = k_b \tan\left(\frac{\theta}{2}\right)\boldsymbol{n}_{ij} \\ \boldsymbol{F}_{jl}^b = k_b \tan\left(\frac{\theta}{2}\right)\boldsymbol{n}_{jl} \\ \boldsymbol{F}_{jj}^b = -(\boldsymbol{F}_{jl}^b + \boldsymbol{F}_{ji}^b) \end{cases} \tag{11}$$

where k_b is the elastic coefficient of the bending spring, θ is the angle between line *ij* and *jl*, $\boldsymbol{n}_{ij}$ and $\boldsymbol{n}_{jl}$ are the unit normal vectors pointed to the outside of the cell. Thus, for particle *j*, the combined spring force is (Ye et al., 2018):

$$\boldsymbol{F}_j = \sum\nolimits_{i,j\ linked} \boldsymbol{F}_{ij}^s + \sum\nolimits_{i,j\ linked} \boldsymbol{F}_{ij}^b \tag{12}$$

Membrane particles are regarded as fluid particles in the spring network model of RBC membrane and participate in the solution of Navier–Stokes equation. The membrane elastic force is added in the source term of the discretized Navier–Stokes equation (Imai et al., 2010):

$$\frac{D\boldsymbol{u}_j}{Dt} = -\frac{1}{\rho}\nabla P + \nu\nabla^2\boldsymbol{u}_j + \boldsymbol{f}_j + \frac{\boldsymbol{F}_j}{\rho V_0} \tag{13}$$

2.3. Iteration format of speed prediction step

The micro scale of the microvasculature makes Reynolds number very small, thus the diffusion term in velocity prediction step is often very large, resulting in divergence. To avoid this, the time step has to be extremely small, increasing the computational burden. The traditional iteration format of velocity estimation step is shown in formula (14), (15), where *k* is the current time step.

$$\boldsymbol{u}^* = \boldsymbol{u}_k + \boldsymbol{f}_k \Delta t \tag{14}$$

$$\boldsymbol{u}^{**} = \boldsymbol{u}^* + \nu\nabla^2\boldsymbol{u}^*\Delta t \tag{15}$$

Imai et al. (2010) have proposed an improved iteration format, in which a smaller time step is used only in calculating Laplacian operator terms, avoiding the problem of excessive value of diffusion terms and not occupying too much computing resources. The iteration format is shown in formulas (16), (17) and (18).

$$\boldsymbol{u}^{*,1} = \boldsymbol{u}^* + \nu\nabla^2\boldsymbol{u}^*\Delta\tau \tag{16}$$

$$\boldsymbol{u}^{*,m+1} = \boldsymbol{u}^{*,m} + \nu\nabla^2\boldsymbol{u}^{*,m}\Delta\tau \tag{17}$$

$$\boldsymbol{u}^{**} = \boldsymbol{u}^{*,M} \tag{18}$$

where the original time step Δt is divided into *M* micro-steps, thus $\Delta\tau = \Delta t/M$. In each $\Delta\tau$, the Laplace operator value of the current velocity is calculated once and accumulated to get the Laplace operator value of the internal velocity. This format is adopted in this paper.

2.4. Model parameter setting and initial arrangement of particles

In this paper, a two-dimensional straight vessel model is established, and its geometric parameters are shown in Fig. 2. The length of the vessel *L* is 80μm and the diameter of the vessel *D* is 10μm. Initially, the RBC is placed 16μm away from the beginning. The inlet velocity u_0 is a constant of 0.005m/s (Sun et al., 2013, 2014), the right end is a zero-pressure outlet, and the upper and lower walls are non-slippery rigid walls. The plasma and the RBC are discretized into fluid particles with average spacing d_0 of 4×10^{-7}m, and the interaction range of the kernel function d_1 is $2.1d_0$.

As for the parameters of plasma (Xiang et al., 2017), the plasma density ρ is 1×10^3kg/m^3 and kinematic viscosity ν is 1×10^{-6}m^2/s. The intracellular fluid properties of RBCs are the same as those of plasma. For the elasticity coefficient of RBCs, Imai et al. (2010) recommends that k_s should be 1×10^{-5}N/m, k_b should be 2.4×10^{-11}N. Since force is often expressed implicitly by acceleration in MPS method, and a single particle weight ρV_0 is 6.4×10^{-17}kg in essay (Imai et al., 2010), rewrite k_s and k_b into acceleration form:

$$k_s = \frac{1 \times 10^{-5}\text{N/m}}{6.4 \times 10^{-17}\text{kg}} = 1.5625 \times 10^{11}\text{s}^{-2} \tag{19}$$

$$k_b = \frac{2.4 \times 10^{-11}\text{N}}{6.4 \times 10^{-17}\text{kg}} = 3.750 \times 10^{5}\text{m/s}^2 \tag{20}$$

For the arrangement of RBCs, essays (Tsubota and Wada, 2010; Wada and Kobayashi, 2003) point out that in the spring network model, biconcave-shaped RBCs can be obtained from spherical RBCs after volume contraction. Based on this, circular cell membranes with diameter of 6.36 μm and intracellular fluids accounting for 50% of the volume of the circle are arranged in the flow field, and the biconcave-shaped RBCs are adaptively obtained by the pressure of the fluid in the solution.

2.5. Verification with plasma Poiseuille flow

In order to verify the accuracy of the MPS method used in this paper, the two-dimensional Poiseuille flow of pure plasma is simulated.

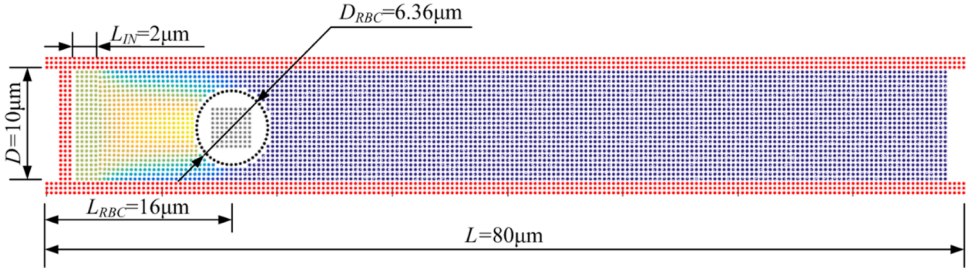

Fig. 2. Diagram of particle initial arrangement.

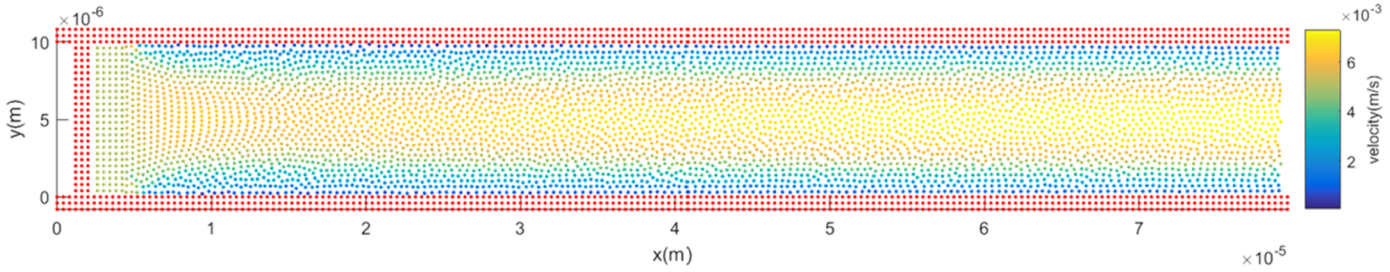

Fig. 3. Velocity distribution in poiseuille flow solved by MPS method.

The flow field with a simulation time of 0.0225s is compared with the analytical solution of Poiseuille flow. The velocity distribution of the simulated flow field is shown in Fig. 3.

The analytical result of small-scale laminar Poiseuille flow Zhang, 2010) points out that the velocity at the center of the fully developed region is 1.5 times that of the inlet velocity, and the velocity profile is parabolic. The mathematical expression is shown in formula ((21):

$$u_x(y) = 1.5 \times u_0 \times \left[\left(\frac{y}{r} - 1\right)^2 + 1\right] \tag{21}$$

where the velocity of entrance $u_0$is constant and r is the radius of the vessel. In order to ensure that the flow is fully developed, the fluid particles in the area range from 64μm to 76μm away from the front edge (dotted line area in Fig. 3) are taken to verify the accuracy of the MPS method. The velocity distribution image in the y direction is shown in Fig. 4.

Formula (16) is used to quantitatively evaluate the difference between the solution solved by MPS method and the analytical solution Li, 2010). It can be found that the relative deviation ε_r between the result given by MPS method and that calculated by formula ((21) is 3.66%.

$$\varepsilon_r = \frac{\sum_{i\in N}\left|\frac{u_{x,i} - u_x(y)}{u_x(y)}\right|}{\sum_{i\in N} 1} \tag{22}$$

3. Results and discussion

3.1. Simulation of a single cell in a straight blood vessel

Firstly, the flow field and the deformation characteristic of RBC are

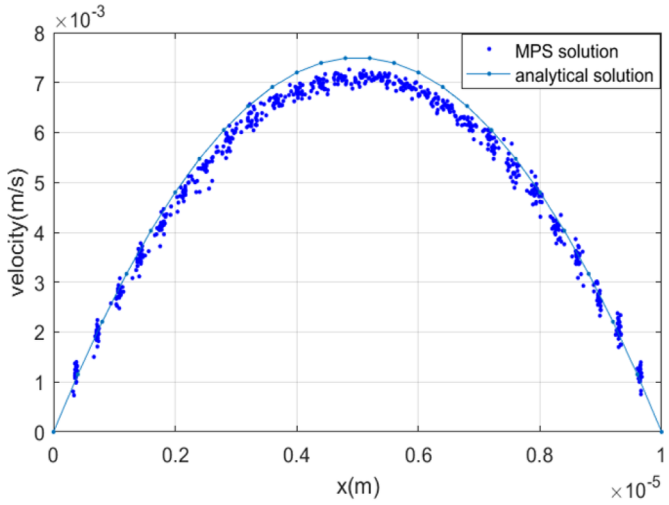

Fig. 4. Radial velocity distribution in poiseuille flow solved by MPS method.

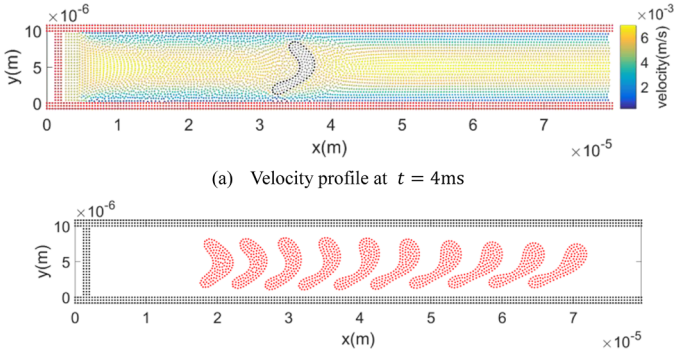

(a) Velocity profile at t = 4ms

(b) Shape and position of RBC from t = 1ms to t = 10ms

Fig. 5. Movement of a single RBC in a straight blood vessel (a) Velocity profile at t = 4ms; (b) Shape and position of RBC from t = 1ms to t = 10ms.

simulated when a single RBC flows through a straight blood vessel. Time step Δt is set to 5×10^{-7}s (Kamada et al., 2010), and the total simulation time is set to 10ms. Shown in the Fig. 5(a) is the velocity profile in the blood vessel at 4ms. The position and shape of the RBC is plotted from t = 1ms to t = 10ms, and the plotting interval is 1ms. The obtained RBC moving image is shown in Fig. 5(b).

It is known from Fig. 5 that the RBC first forms an axisymmetric parachute shape by the flushing of the inlet flow, and then the tank-treading motion occurs as the cell moves forward. This paper further simulates a RBC flowing through straight microvessels where semicircular thrombi of different sizes are placed on the wall. A semicircular thrombus with the radius r_T of $4 \times d_0$ or $8 \times d_0$ is placed 32μm from the anterior edge of the vessel.

Fig. 6 depicts the flow field velocity profile and the deformation of a RBC at a thrombus radius of $r_T = 4 \times d_0$. It can be seen that the flow area becomes smaller and the flow velocity becomes higher around the thrombus, thus the cell has to fold to pass through the thrombus region,

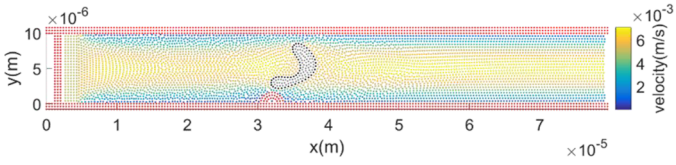

(a) Velocity profile at t = 4ms

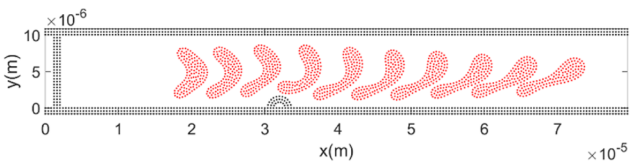

(b) Shape and position of RBC from t = 1ms to t = 10ms

Fig. 6. Movement of a single RBC in a straight blood vessel, where a $4 \times d_0$thrombus is placed. (a) Velocity profile at t = 4ms; (b) Shape and position of RBC from t = 1ms to t = 10ms.

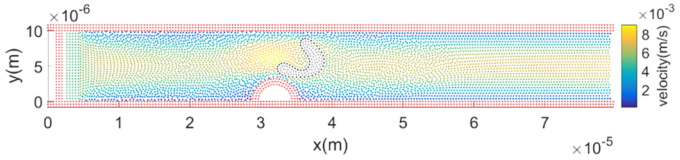

(a) Velocity profile at $t = 4$ms

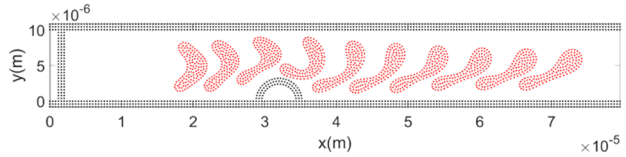

(b) Shape and position of RBC from $t = 1$ms to $t = 10$ms

Fig. 7. Movement of a single RBC in a straight blood vessel, where a $8 \times d_0$thrombus is placed. (a) Velocity profile at $t = 4$ms; (b) Shape and position of RBC from $t = 1$ms to $t = 10$ms.

as shown in Fig. 6(b). After passing through this area, the RBC returns to their original shape due to the elasticity of the cell membrane. Fig. 7 shows the flow field velocity profile and the deformation of a RBC at a thrombus radius of $r_T = 8 \times d_0$. According to Figs. 6 and 7, as the size of the thrombus increases, the RBC undergoes greater deformation when passing by the thrombus.

In order to quantitatively analyze the cell deformation, a deformation factor τ is introduced based on the moment of inertia of the cell, as shown in the formula (23). In the formula, I_{1ini} and I_{2ini} are the moment of inertia in the initial state.

$$\tau = \frac{(I_1^2 + I_2^2)^{1/2}}{(I_{1ini}^2 + I_{2ini}^2)^{1/2}} \tag{23}$$

The curve of the deformation factor is shown in Fig. 8. It can be seen from the figure that when the cell moves toward the thrombus, the deformation factor is smaller than that without the thrombus, and such reduction becomes more significant as the thrombus becomes larger. This is because the blood cell starts to fold when it moves towards the thrombus, resulting in a shape that is closer to a sphere. The most significant position of the reduction happens at $x = 35\mu$m, where the $r_T = 8 \times d_0$ thrombus causes the cell deformation factor to decrease by 17.23% compared with no thrombus. After passing the thrombus, the deformation factor of the cell returns to a higher value because of the re-stretching of the cell. The most obvious position of the deformation recovery is $x = 44\mu$m, where the deformation factor of the cell affected

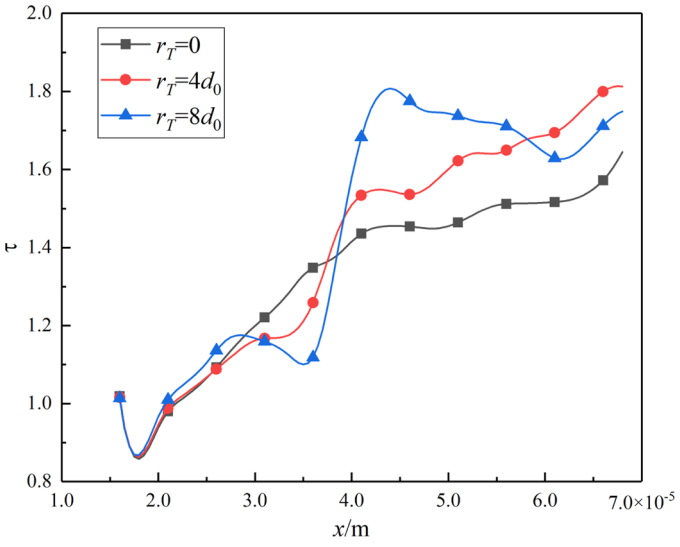

Fig. 8. The deformation factor of the cell.

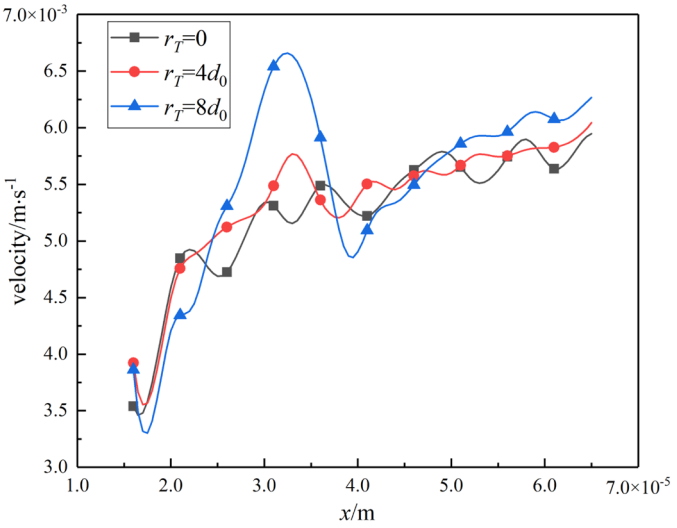

Fig. 9. Axial velocity of the RBC.

by the $r_T = 8 \times d_0$ thrombus increases by 24.19% compared with no thrombus.

The axial velocity of the RBC is shown in Fig. 9. When passing through the thrombus area, the axial velocity of the RBC appears to increase significantly. Under the presence of the $r_T = 4 \times d_0$ thrombus, the velocity reaches its peak value of 6.0×10^{-3}m/s, whichis 15.4% larger than that without thrombus. When a $r_T = 8 \times d_0$ thrombus exists, the peak value of velocity is further increased to 7.2×10^{-3}m/s, which is 38.5% larger than that without thrombus. Therefore, as the size of the thrombus increases, the axial velocity increases accordingly when the RBC passes through the thrombus region.

3.2. Simulation of two side-by-side RBCs in a straight blood vessel

A straight vessel containing two RBCs is further examined, and its geometrical parameters are shown in Fig. 10. The vessel length L is 120μm ($300 \times d_0$), and the diameter D is 20μm ($50 \times d_0$). Initially, two RBCs are symmetrically arranged at x = 16μm. The inlet at the left edge provides a constant inlet velocity $u_0 = 0.005$ m/s, and the right end is a zero-pressure outlet.

Time step Δt is still set to 5×10^{-7}s, but the total simulation time is increased to 15ms because of the longer vessel. The position and shape of the RBCs are plotted from $t = 2$ms to $t = 14$ms, and the plotting interval is 2ms. The obtained RBC moving image is shown in Fig. 11.

According to Fig. 11, two RBCs show little parachute motion trend, but gradually incline and start tank treading motion because of the radial velocity gradient of the Poiseuille flow. Also, as the velocity is faster near the axis, the cells are elongated as they move. This paper further calculates the movement and deformation characteristics of RBCs where two thrombi are placed in the blood vessel. Two thrombi with radius r_T of $12 \times d_0$ are arranged on both sides of the flow channel. The thrombus on the lower side is located at $x = 150 \times d_0$.The upper side thrombus is firstly also placed at $x = 150 \times d_0$, but a cascade of situations where the upper thrombus moves rightward at the interval of $10 \times d_0$ is investigated, the axial distance of the two thrombi Δ_T increases from $10 \times d_0$ to $70 \times d_0$, as shown in Fig. 12.

As can be seen from Fig. 12, when the two thrombi are simultaneously placed at $x = 150 \times d_0$, the flow path is significantly narrowed, causing one of the cells to lag behind the other. When the upper thrombus moves $10 \times d_0$ rightward, the two cells can pass the thrombus almost simultaneously, but undergo significant deformation. As the upper thrombus continues to move rightward, the deformation of the cells is reduced, and the combined effect of the two thrombi is no longer apparent. Finally, when the distance Δ_T reaches $70 \times d_0$, as

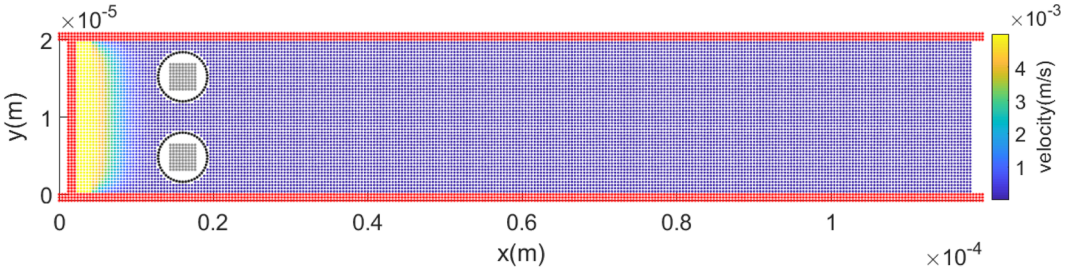

Fig. 10. Initial particle layout of two side-by-side RBCs in a straight blood vessel.

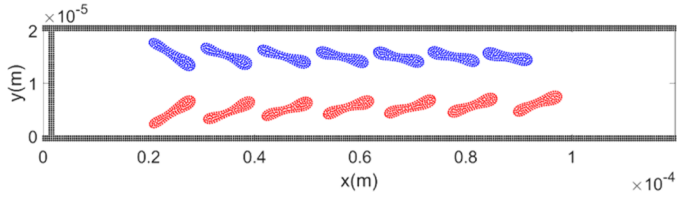

Fig. 11. Movement of two parallel RBCs in a straight blood vessel.

shown in Fig. 12(h), the two thrombi are almost independent.

Quantitative analysis of the velocity and deformation is induced on the two RBCs. Firstly, the curve of the axial velocity is shown in Fig. 13.

From Fig. 13, it is known that for the lower cell, a velocity peak appears between 60μm and 70μm, which indicates that the velocity is mainly affected by the lower thrombus. Moreover, as the upper thrombus moves rightward, the velocity peak value decreases accordingly, indicating the reduction of the combined effect of the two thrombi. For the upper cell, the position of the maximum velocity moves with the upper thrombus, and the velocity curve generally decreases with the right shift of the upper thrombus, indicating that the moving velocity of the upper cell is mainly affected by the upper thrombus, and the reduction of the combined effect also influences the upper cell.

Fig. 14 quantitatively describes the effect of the upper thrombus position on the peak velocity. The peak velocity of both cells decreases significantly as the upper thrombus moves rightward. When the axial distance between the two thrombi Δ_T increases from $0 \times d_0$ to $70 \times d_0$, the peak velocity of the lower cell decreases from 0.0106 m/s to 0.0073 m/s, about 31.5%; the peak velocity of the upper cell decreases from 0.0095 m/s to 0.0071 m/s, about 24.6%.

The deformation factors of the two cells with their axial

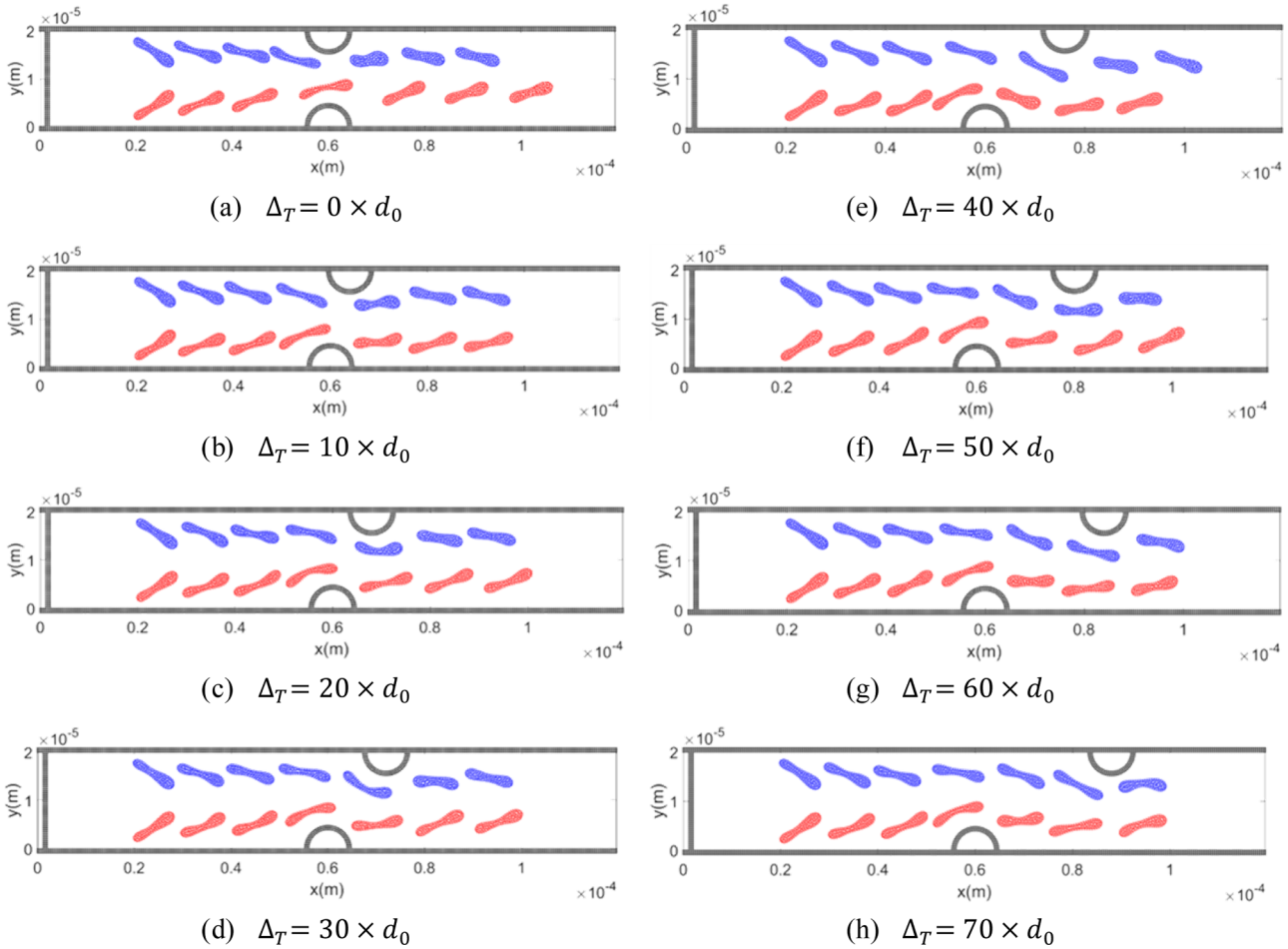

Fig. 12. Movement of two parallel RBCs in a straight blood vessel with two thrombi on the different side. (a) $\Delta_T = 0 \times d_0$; (b) $\Delta_T = 10 \times d_0$; (c) $\Delta_T = 20 \times d_0$; (d) $\Delta_T = 30 \times d_0$; (e) $\Delta_T = 40 \times d_0$; (f) $\Delta_T = 50 \times d_0$; (g) $\Delta_T = 60 \times d_0$; (h) $\Delta_T = 70 \times d_0$.

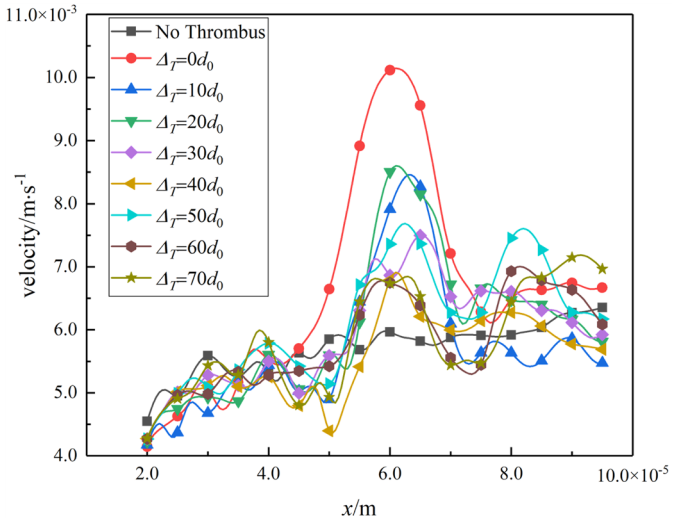

(a) Axial velocity of the lower RBC.

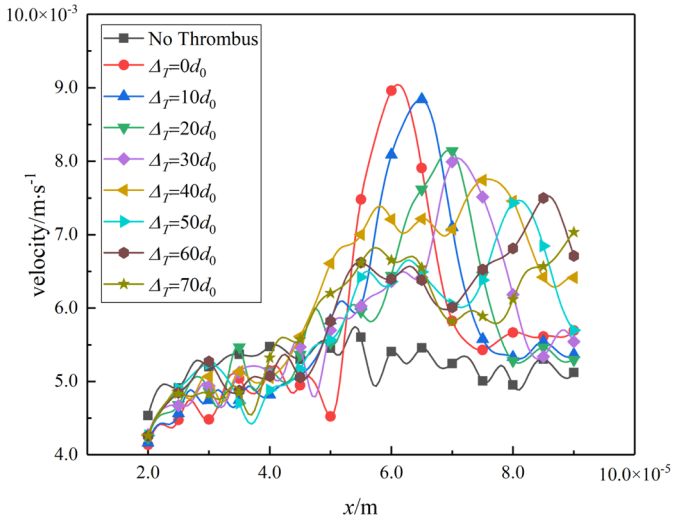

(b) Axial velocity of the upper RBC.

Fig. 13. Axial velocity of the two RBCs in a straight blood vessel. (a) Axial velocity of the lower RBC.; (b) Axial velocity of the upper RBC.

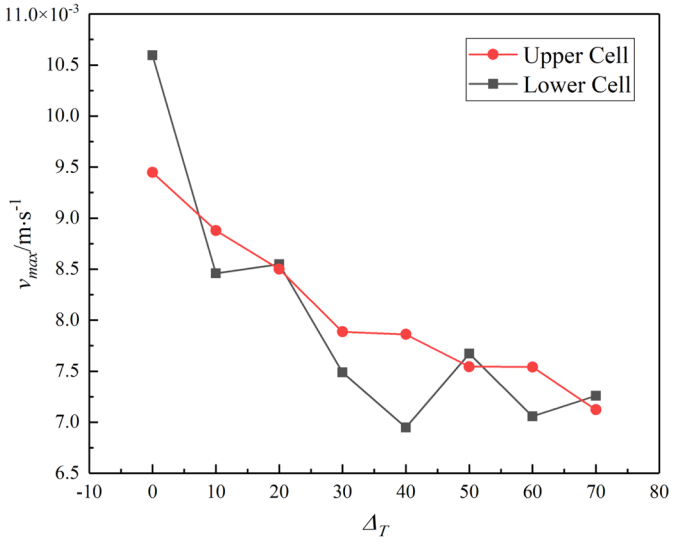

Fig. 14. The effect of the thrombi distance on the peak velocity.

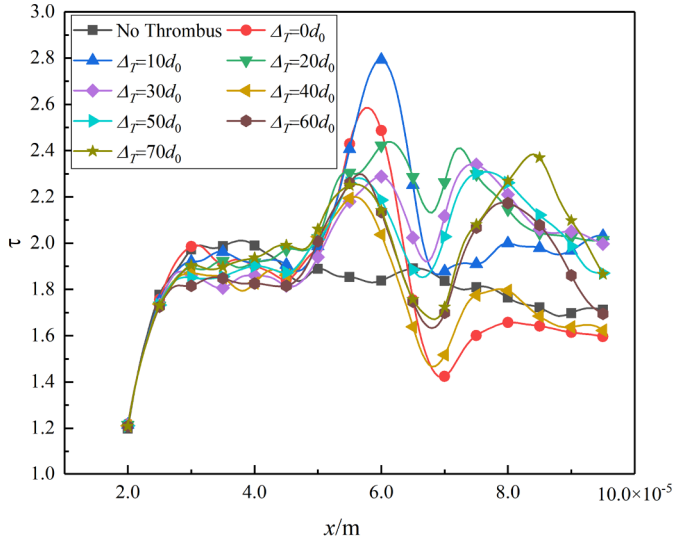

(a) Deformation factor of the lower cell.

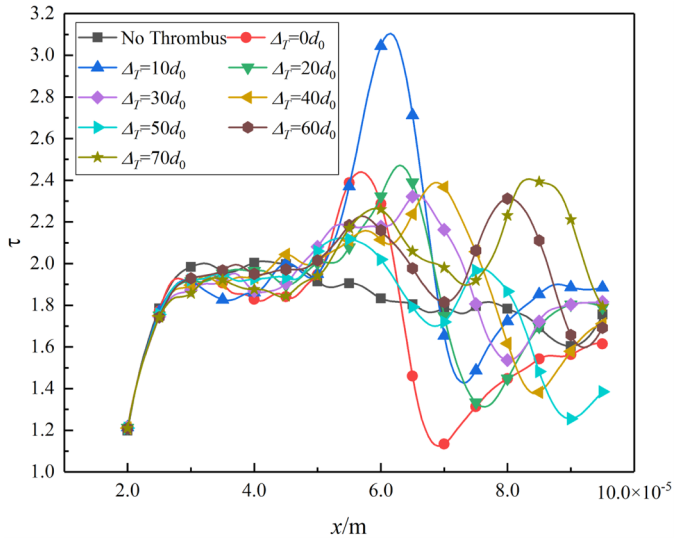

(b) Deformation factor of the upper cell.

Fig. 15. Deformation factor of the two RBCs in a straight blood vessel. (a) Deformation factor of the lower cell. (b) Deformation factor of the upper cell.

displacement are shown in Fig. 15. Unlike a single blood cell shown in 3.1, in the case where two RBCs are placed side by side in the blood vessel, the RBCs basically move along the long axis direction when passing through the blood clot, so that they do not fold due to the pressing. It can be seen from Fig. 15 that the RBCs no longer have a reduced deformation factor before passing through the thrombus. Instead, the peak of the deformation factor directly appears because of the gradually narrowed flow path. After passing the thrombus, the high-speed blood flow impact and thrombus compression of the cells are rapidly weakened, and the cells are contracted by the tension of the cell membrane, so that the deformation amount is lower than that without the thrombus.

For the lower cell, although the flow path is the narrowest when the two thrombi have the same axial position, since the two cells pass through the thrombus in succession, the deformation factor has a relatively lower value. When the distance Δ_T is slightly increased to $10 \times d_0$, the flow path is narrow and the cells passed side by side. Therefore, the peak value of the deformation factor reaches 2.79, which is the highest. As the upper thrombus moves further to the right, the peak of the deformation factor is further reduced. The relatively lower

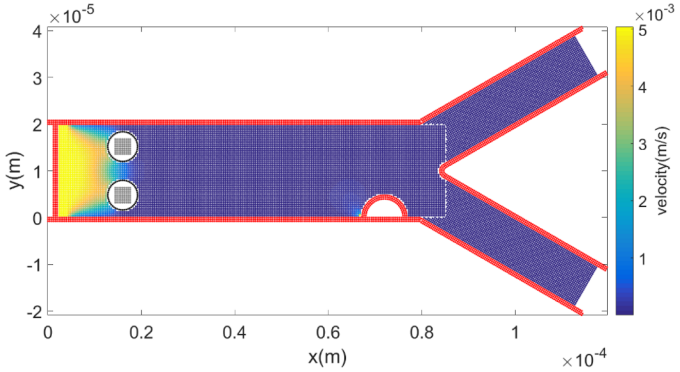

Fig. 16. Initial particle layout of two side-by-side RBCs in a bifurcated vessel.

deformation factor where axial distance is 40 × d_0, which is also caused by the sequential passage of the cells.

For the upper cell, the position of the deformation peak value moves rightward along with the upper thrombus. When the distance Δ_T is 10 × d_0, the peak value of the deformation is the largest, reaching 3.10.

3.3. Simulation of two side-by-side RBCs in a bifurcated vessel

Bifurcated blood vessels are also very common in human's circulatory system. In this paper, a bifurcated vessel model with two RBCs is established. The model consists of a 20μm diameter vessel with a length of 80μm (200 × d_0) and two 10μm diameter vessels with 40μm long, as shown in Fig. 16. The thrombus is placed at $x = 72\mu$m.

The deformation characteristics of RBCs in the bifurcated vessel are calculated when the thrombus radius r_T is 8 × d_0, 12 × d_0, 16 × d_0 and 20 × d_0, respectively. Time step Δt is set to 5×10^{-7}s, and the total simulation time is set to 15ms. The position and shape of the RBCs are plotted from $t = 2$ms to $t = 14$ms, and the plotting interval is 2ms. The obtained RBC moving images are shown in Fig. 17.

The curve of the lower cell velocity is shown in Fig. 18(a). It can be seen that in the case without thrombus, the lower cell tends to accelerate slowly as it flowing through the blood vessel. However, when a thrombus exists, the velocity of the lower cell reaches its peak near the thrombus. As the diameter of the thrombus increases, the maximum velocity of the cell increases accordingly. For the upper cell shown in Fig. 18(b), since it is far from the thrombus, its speed does not increase such significantly as the lower cell.

Fig. 19 shows the velocity of two cells at the midline of the thrombus, where $x = 72\mu$m. Although the velocity of the upper cell increases slower with the diameter increasing of the thrombus, when the radius of the thrombus reaches 20 × d_0, the velocity of the upper cell increases significantly. This is because the thrombus is large enough, so that the lower cell is blocked by the thrombus, thus the upper cell passes the thrombus earlier. At this time, the compression of the upper cell becomes smaller, and it is able to enter the middle part of the flow channel where the flow speed is the fastest. When the radius of the upper thrombus increases from 0 × d_0 to 20 × d_0, the peak velocity of the lower cell increases from 0.0056 m/s to 0.0085 m/s, a total increase of 51.6%; and the peak velocity of the upper cell increases from 0.0053 m/s to 0.0089 m/s, a total increase of 67.9%.

The deformation factor of the two cells is shown in Fig. 20. For the lower cell, when no thrombus exists, the deformation factor of the lower cell remains almost the same. In the presence of a thrombus, the deformation factor peaks at the position of the front edge of the thrombus, and the peak value increases as the radius of the thrombus increases. This is because when the cell passes through the leading edge of the thrombus, the front side of the cell is closer to the narrowest point of the flow channel, and the fluid impact is stronger than the rear side of the cell, causing the cell to elongate. After passing through the midline of the thrombus, the flow channel suddenly expands and the flow rate becomes slower, thus the cell shrinks rapidly due to the elastic force of the cell membrane, so that the deformation factor is lower than that without thrombus.

For the upper cell, when no thrombus exists, the deformation factor of the upper cell also remains almost the same. In the presence of a thrombus, however, although the upper cell also shows a peak in the deformation factor at the front edge of the thrombus, the deformation factor of the upper cell undergoes much smaller reduction than that of the lower cell after passing through the midline of the thrombus. This is because the upper bifurcation vessel has a significantly higher flow rate than the lower bifurcation vessel because there is no blockage at the inlet. When the upper cell moves to the rear side the thrombus, its front side enters the upper bifurcation vessel where fluid velocity is high, thus the deformation factor of the cell begins to rise again. Besides, when the thrombus radius reaches 20 × d_0, the peak deformation of the upper cell is lower, because when the thrombus is large enough, the lower cell is blocked by the thrombus, and its movement speed is significantly slower, making the upper cell flow through the thrombus earlier, thereby avoiding compression with the lower cell.

4. Conclusion

In this paper, MPS method and the spring network model of RBC membrane are used to study the movement and deformation of RBC in two-dimensional straight and bifurcated blood vessels.

The simulation of the movement and deformation of RBCs in straight microvasculature shows that RBCs will not only be parachute shaped, but also have a tank-treading motion with blood flow. Simulation of the movement of a single RBC with thrombus shows that, compared with the case without thrombus, the deformation of RBCs decreases by 17.23% and then increases by 24.19% when passing thrombus with radius in8 × d_0. This indicates that a single RBC will be compressed and folded because of thrombus first, which reduces the deformation factor. After passing the thrombus, the RBC will stretch again and the deformation will rise to higher value. At the same time, when the thrombus radius is 4 × d_0 and 8 × d_0, the maximum speed of RBCs passing through these vessels increases by 15.4% and 38.5% respectively, which indicates that the presence of thrombus will increase the velocity of RBCs and induce greater squeezing effect on them. The larger the thrombus is, the more significant the influence on the movement and deformation of RBCs will be.

The simulation of two RBCs in the straight microvasculature shows that when the RBCs are not located in the middle of the blood vessel, the cells will more tend to undertake tank-treading motion than just forming parachute shapes. After placing thrombi on both sides of the blood vessel, the simulation shows that RBCs is not folded like a single RBC when entering the thrombus area, but directly elongated by higher blood flow rate; after passing through the thrombus area, the influence induced by thrombi disappears and the cells start bouncing back to the original shape. Therefore, the deformation of RBCs increases first and then decreases. At the same time, the simulation results show that the two RBCs can only pass through the thrombus successively when the two thrombi with radius of 12 × d_0 are located in the same position, although the RBCs move the fastest at this time, the deformation of RBCs is not the greatest. When the axial positions of the two thrombi are10 × d_0 different, the RBCs can just pass through the thrombi at the same time, thus the deformation of RBCs reaches the maximum value of 3.10 and 2.79, respectively. Later, as the two thrombi moved further away, the maximum deformation of RBCs decreased, and the combined effect of the two thrombi is weakened. When the distance between the two thrombi is increased to 70 × d_0, the effect on RBCs is equivalent to that caused by two independent thrombi.

The simulation of two RBCs passing side by side through the bifurcated blood vessel with no thrombus on the wall shows that the two RBCs enter the two bifurcated vessels respectively, and the deformation remains basically unchanged after the beginning. However, when the

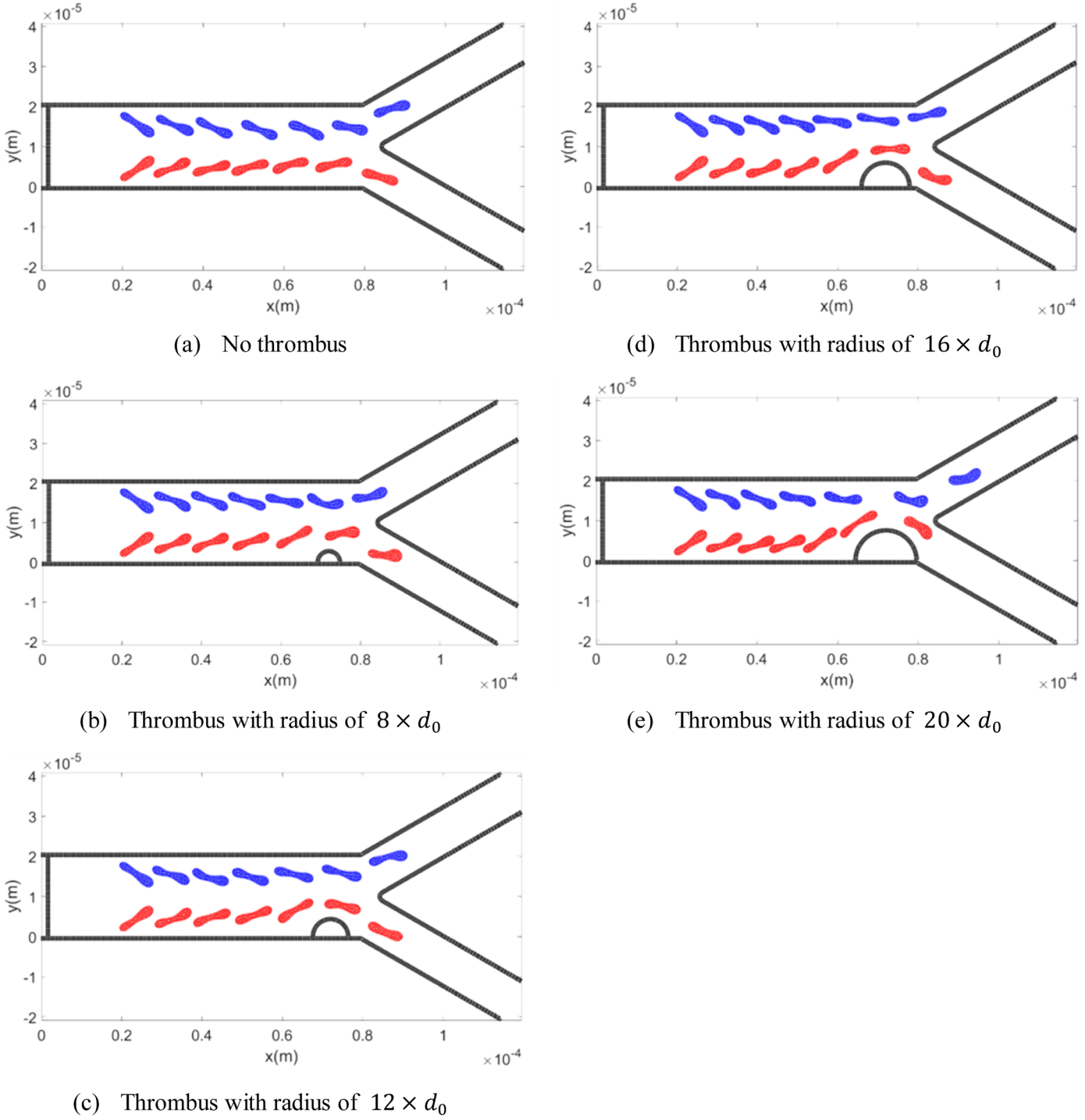

Fig. 17. Movement of two parallel RBCs in a bifurcated vessel with thrombi of different sizes. (a) No thrombus; (b) Thrombus with radius of 8 × d_0; (c) Thrombus with radius of 12 × d_0; (d) Thrombus with radius of 16 × d_0; (e) Thrombus with radius of 20 × d_0.

RBC passes through the thrombus, its front part is closer to the narrowest part of the blood vessel, the impact of the fluid is stronger than the rear part of the RBCs, resulting in the elongation of the RBCs, so their deformation factors reach the peak value at the front side of the thrombus. After the RBC passes through the middle line of the thrombus, the flow slows down suddenly, and the RBCs shrink rapidly due to the elasticity of the cell membrane, resulting in smaller deformation factors compared with the situation of no thrombus. When the thrombus increases gradually, the two RBCs still enter the two bifurcated vessels, and the movement and deformation of the RBC near the thrombus are greatly affected by the thrombus. With the increase of thrombus diameter, the maximum velocity and deformation of both RBCs increased, and the maximum velocity and deformation factor of RBC near the thrombus increased faster than those of other RBCs. When the diameter of the thrombus is large enough, the lower RBC will be blocked by the thrombus, which lags behind the upper RBC, so that the upper RBC undergoes relatively slighter squeeze and flows faster. The simulation shows that when the radius of the thrombus reaches20 × d_0, the maximum velocity of the RBC near the thrombus rises significantly, even becomes larger than the maximum velocity of another RBC, accordingly, the peak deformation decreases. When the radius of the thrombus changed from 0 × d_0 to 20 × d_0, the peak velocities of the

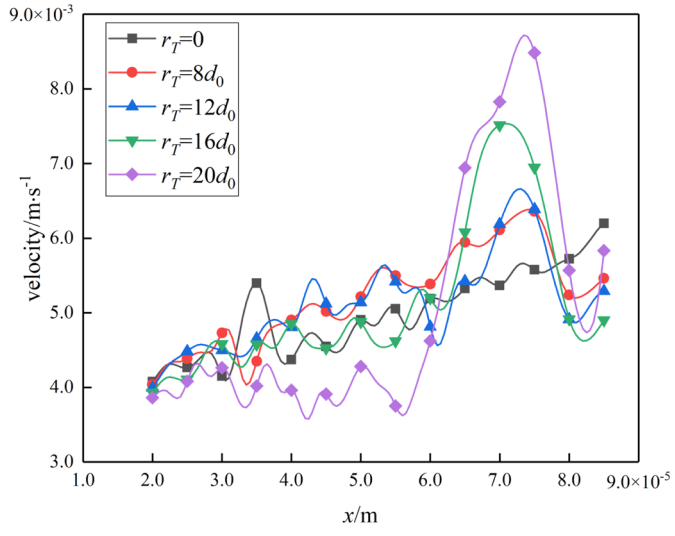

(a) Axial velocity of the lower cell.

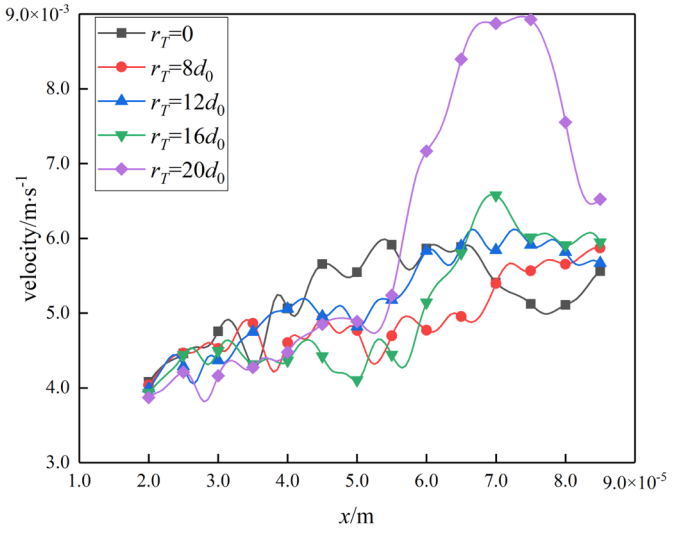

(b) Axial velocity of the upper cell.

Fig. 18. Axial velocity of the two RBCs in a bifurcated blood vessel. (a) Axial velocity of the lower cell; (b) Axial velocity of the upper cell.

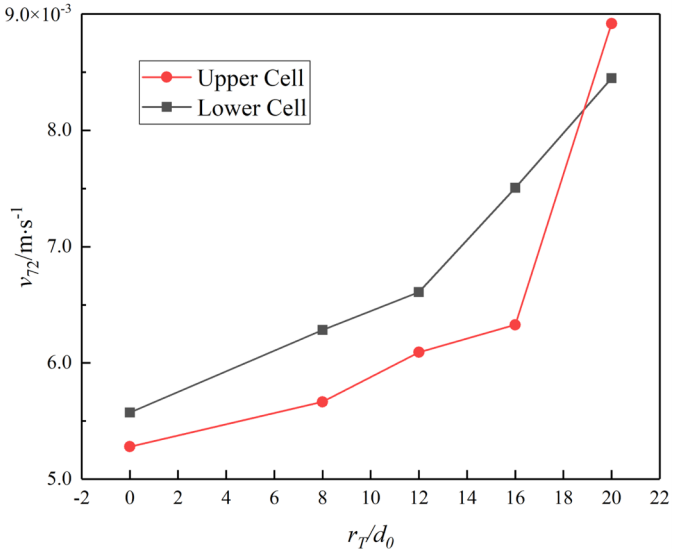

Fig. 19. The speed of the two cells at $x = 72\mu$m.

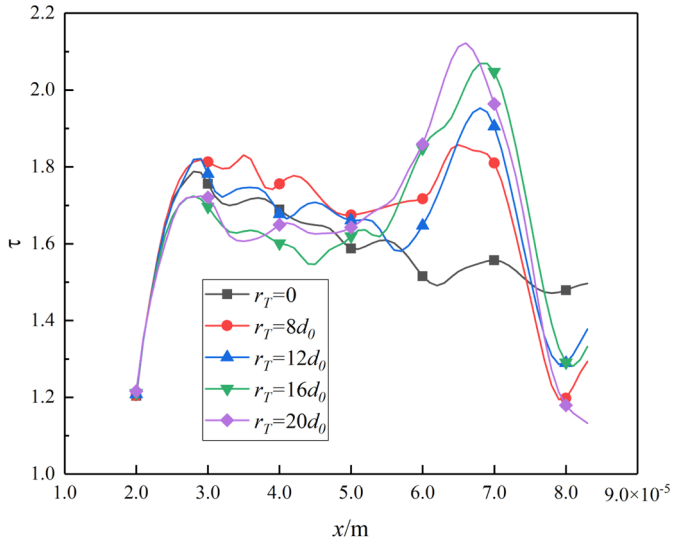

(a) Deformation factor of the lower cell.

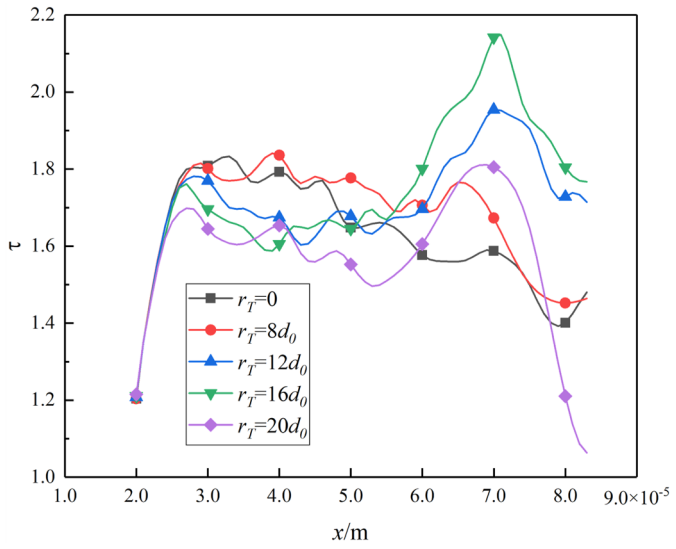

(b) Deformation factor of the upper cell.

Fig. 20. Deformation factor of the two RBCs in a bifurcated blood vessel. (a) Deformation factor of the lower cell; (b) Deformation factor of the upper cell.

upper and lower cells increased by 51.6% and 67.9%, respectively.

Acknowledgements

This work has been supported by the National Natural Science Foundation of China (Grant number 51876161).

Supplementary materials

Supplementary material associated with this article can be found, in the online version, at doi:10.1016/j.ijheatfluidflow.2019.108520.

Reference

Ahmadian, M.T., Firoozbakhsh, K., Hasanian, M, 2012. Simulation of red blood cell motion in microvessels using modified moving particle semi-implicit method. Scientia Iranica 19, 113–118.
Balogh, P., Bagchi, P., 2017. A computational approach to modeling cellular-scale blood flow in complex geometry. J. Comput. Phys. 334, 280–307.
Di Achille, P., Humphrey, J.D., Tellides, G., 2017. Hemodynamics-driven deposition of intraluminal thrombus in abdominal aortic aneurysms. Int. J. Numer. Method Biomed. Eng. 33.

Discher, D.E., Boal, D.H., Boey, S.K., 1998. Simulations of the erythrocyte cytoskeleton at large deformation. II. Micropipette aspiration. Biophys. J. 75, 1584–1597.
Dzwinel, W., Boryczko, K., Yuen, D.A., 2003. A discrete-particle model of blood dynamics in capillary vessels. J. Colloid Interface Sci. 258, 163–173.
Fedosov, D.A., Caswell, B., Karniadakis, G.E., 2010. A multiscale red blood cell model with accurate mechanics, rheology, and dynamics. Biophys. J. 98, 2215–2225.
Gambaruto, A.M., 2015. Computational hemodynamics of small vessels using the moving particle semi-implicit (MPS) method. J. Comput. Phys. 302, 68–96.
Harada, T., Suzuki, Y., Koshizuka, S., Arakawa, T., Shoji, S, 2007. Simulation of droplet generation in micro flow using MPS method. JSME Int. J. Ser. B Fluids Therm Eng 49, 731–736.
Hosseini, S.M., Feng, J.J., 2009. A particle-based model for the transport of erythrocytes in capillaries. Chem. Eng. Sci. 64, 4488–4497.
Imai, Y., Kondo, H., Ishikawa, T., Lim, C.T., Yamaguchi, T., 2010. Modeling of hemodynamics arising from malaria infection. J. Biomech. 43, 1386–1393.
Imai, Y., Omori, T., Ishikawa, T., Shimogonya, Y., Yamaguchi, T., 2016. Numerical methods for simulating blood flow at macro, micro, and multi scales. J. Biomech. 49, 2221–2228.
Jared, O.B., Jonathan, P.A., Juan, M.R., Timothy, W.S., 2008. Simulated two-dimensional red blood cell motion, deformation, and partitioning in microvessel bifurcations. Ann. Biomed. Eng. 10, 1690.
Kamada, H., Imai, Y., Nakamura, M., Ishikawa, T., Yamaguchi, T., 2012. Computational analysis on the mechanical interaction between a thrombus and red blood cells: possible causes of membrane damage of red blood cells at microvessels. Med. Eng. Phys. 34, 1411–1420.
Kamada, H., Tsubota, K., Nakamura, M., Wada, S., Ishikawa, T., Yamaguchi, T., 2010. A three-dimensional particle simulation of the formation and collapse of a primary thrombus. Int. J. Numer. Method Biomed. Eng. 26, 488–500.
Koshizuka, S., Nobe, A., Oka, Y., 2015. Numerical analysis of breaking waves using the moving particle semi-implicit method. Int. J. Numer. Methods Fluids 26, 751–769.
Koshizuka, S., Oka, Y., 1996. Moving-Particle semi-implicit method for fragmentation of incompressible fluid. Nucl. Sci. Eng. 123, 421–434.
Li, F., Hu, R.Q., Yamada, T., He, Y., Ono, N., 2014. The observations of the flow behavior and distribution of red blood cells flowing through a micro-network channel. Chin. J. Theor. Appl. Mech. 46, 1–9.
Li, Y.Z, 2010. Thermal and Power Mechanical Testing Technology. Xi'an Jiaotong University Press, Xi'an.
Liu, Y., Liu, W.K., 2006. Rheology of red blood cell aggregation by computer simulation. J. Comput. Phys. 220, 139–154.
Mohandas, N., Gallagher, P.G., 2008. ASH 50th anniversary review red cell membrane: past, present, and future. Blood 112, 3939–3948.
Nakamura, M., Bessho, S., Wada, S., 2014. Analysis of red blood cell deformation under fast shear flow for better estimation of hemolysis. Int. J. Numer. Method Biomed. Eng. 30, 42–54.
Pries, A.R., Ley, K., Claassen, M., Gaehtgens, P., 1989. Red cell distribution at microvascular bifurcations. Microvasc. Res. 38, 81–101.
Schmid-Schönbein, G.W., Usami, S., Chien, S., Skalak, R., 1980. Cell distribution in capillary networks. Microvasc. Res. 19, 18–44.
Sharifi, Alireza, Moghadam, Mohammad Charjouei, 2016. CFD simulation of blood flow inside the corkscrew collaterals of the Buerger's disease. BioImpacts 6, 41.
She, S., Li, Q., Shan, B., Tong, W., Gao, C., 2013. Fabrication of red-blood-cell-like polyelectrolyte microcapsules and their deformation and recovery behavior through a microcapillary. Adv. Mater. 25, 5814–5818.
Sugihara-Seki, M., Fu, B.M., 2005. Blood flow and permeability in microvessels. Fluid Dyn. Res. 37, 82–132.
Sui, Y., Chew, Y.T., Roy, P., Cheng, Y.P., Low, H.T., 2008. Dynamic motion of red blood cells in simple shear flow. Phys. Fluids 20, 112106.
Sun, Z.G., Lan, A.Q., Xi, G., 2014. Numerical simulation of cylindrical liquid jet based on the MPS method. J. Eng. Thermophys. 35, 490–493.
Sun, Z.G., Li, D.C., Chen, X., Liang, Y.Y., Xi, G., 2013. Velocity boundary models of inlet flow using moving particle semi-implicit method. J. Xi'an Jiaotong Univ. 47, 87–91.
Sun, Z.G., Xi, G., Wang H, R., 2008. Numerical simulation of incompressible flow with moving component using the MPS method. J. Eng. Thermophys. 10, 1676–1678.
Sun, Z.G., Xi, G., Xiang, L.F., 2007. Simulation on rising bubble in water with meshfree method. J. Eng. Thermophys. 5, 772–774.
Suzuki, Y., Tateishi, N., Soutani, M., Maeda, N, 1996. Deformation of erythrocytes in microvessels and glass capillaries: effects of erythrocyte deformability. Microcirculation 3, 49–57.
Tsubota, K., Wada, S., Yamaguchi, T., 2006. Particle method for computer simulation of red blood cell motion in blood flow. Comput. Methods Programs Biomed. 83, 139–146.
Tsubota, K.I., Wada, S., 2010. Elastic force of red blood cell membrane during tank-treading motion: consideration of the membrane's natural state. Int. J. Mech. Sci. 52, 356–364.
Wada, S., Kobayashi, R., 2003. Numerical simulation of various shape changes of a swollen red blood cell by decrease of its volume. Trans. Jpn. Soc. Mech. Eng. Ser. A 69, 14–21.
Xiang, H., Chen, B., Ying, C.X., 2017. Numerical simulation of pale thrombus formation in a Y-Bifurcation vessel with the MPS method. J. Eng. Thermophys. 38, 2367–2371.
Xiao, L.L., Chen, S., Liu, J.Y., Shang, Z., 2013. Coarse-grained simulation of red blood cells stretching deformation. J. Tongji Univ. (Nat. Sci.) 41, 1744–1750.
Ye, T., Phan-Thien, N., Lim, C.T., Li, Y., 2017. Red blood cell motion and deformation in a curved microvessel. J. Biomech. 65, 12–22.
Ye, T., Shi, H., Li, Y., Phan-Thien, N., Lim, C.T., 2018. Relationship between transit time and mechanical properties of a cell through a stenosed microchannel. Soft Matter 14, 533–545.
Yu, Y.J., Wang, Y., Xu, S.L., 2015. CFD simulation of the two-phase flow of blood and thrombus flow in blood vessels. J. Chem. Eng. Chin. Univ. 29, 992–996.
Zhang, M.Y, 2010. Fluid Mechanics. Higher Education Press, Beijing.